Electrodeposition, Morphology, Composition, and Corrosion Performance of Zn-Mn Coatings from a Deep Eutectic Solvent

S. Fashu, C.D. Gu, J.L. Zhang, H. Zheng, X.L. Wang, and J.P. Tu

Different Zn-Mn coatings were successfully electrodeposited on copper substrates from deep eutectic solvent-based electrolytes containing boric acid as an additive. The main objective of this work was to optimize the Zn/Mn ratios and morphologies of the as-electrodeposited Zn-Mn films in order to obtain better corrosion protection performance coatings. The electrodeposition behaviors of Zn-Mn alloys as studied by cyclic voltammetry showed that with increase in electrolyte Mn(II) concentration, Zn(II) ion reduction occurs at higher overpotentials while Mn reduction occurs at lower overpotentials, and this in turn enhances Mn incorporation into the deposit. Characterization results showed that the electrodeposition potential and electrolyte Mn(II) concentration significantly affects the Mn content, crystal structure, surface morphology, and corrosion performance of the deposits. With increase in electrodeposition potential and electrolyte Mn(II) concentration, the alloy Mn increased and the grain morphology was refined. The crystal structure of Zn-Mn deposits consists of Zn and hexagonal close packed ε-phase Zn-Mn at low electrode-position potentials and low electrolyte Mn(II) content. However, at high electrodeposition potentials and electrolyte Mn(II) contents, the crystal structure was only composed of hexagonal close packed ε-phase Zn-Mn. Corrosion measurements show that all the Zn-Mn samples have a passivating behavior and exhibits higher corrosion resistances when compared to those from aqueous solutions. Thus, optimum electrodeposition potential and electrolyte Mn(II) concentration were determined producing compact Zn-Mn films with the best corrosion resistance.

1. Introduction

The electrodeposition of Zn as an alloy with elements like Fe, Co, Sn, Ni, Mn and Cr is nowadays of great importance not only for corrosion protection of metallic substrates but also in applications such as catalysts, electrodes for batteries, and magnetic uses (Ref 1-13). In the research and improvement on Zn alloy eletrodeposition for sacrificial corrosion protection of metallic substrates, there is a growing interest in the Zn-Mn alloy system. This is because Zn-Mn alloys show synergistic effects, resulting in better corrosion resistances than individual Zn and Mn metals (Ref 3), hence it has been reported that some Zn-Mn alloys exhibit the highest corrosion resistance known among Zn alloys in an aggressive corrosive media (Ref 1, 9, 14). The synergistic effects arise because, Zn-Mn alloy coatings, although being thermodynamically less noble than Zn, combines their sacrificial protection ability with the

formation of a practically insoluble passive barrier surface layer. Another area of interest is the automotive industry which is now trying to replace some steel components with light-weight materials, such as aluminum or magnesium and since Zn-Mn alloys have potentials that are closer to and more active than those of aluminum or magnesium, thus these Zn-Mn alloy coatings have a huge potential for corrosion protection of light weight materials. Zn-Mn alloys can be electrodeposited from a variety of aqueous baths (Ref 2, 8, 9, 12) containing complexing agents which brings Zn and Mn deposition potentials closer. The electrodeposition of Zn-Mn alloys from aqueous baths is complicated mostly because of poor bath stability (due to precipitation of Mn) and intrinsically low current efficiencies, particularly when alloys with high Mn content are required. Low current efficiencies arise because the very negative potentials required for Mn reduction results in significant parallel hydrogen evolution reactions (Ref 15, 16).

It has been reported that Zn-Mn alloy coatings with Mn contents around 15% have a higher corrosion resistance in marine atmosphere than bare Zn or other Zn alloys (Ref 17). Boshkov et al. (Ref 8, 18, 19) studied the influence of alloy composition on the corrosion behavior of Zn-Mn alloy coatings and reported that monophasic Zn-Mn alloy coatings with Mn contents around 11% posses the highest corrosion resistance due to their crystal structure and a sufficiently higher Mn content. Gabe (Ref 2) reported that Zn-Mn alloys with Mn contents of approximately 30% exhibit the highest corrosion resistance and this was also attributed to their crystal structure and high Mn composition. Recently, Muller et al. (Ref 20, 21)

S. Fashu, C.D. Gu, J.L. Zhang, H. Zheng, X.L. Wang, and J.P. Tu, State Key Laboratory of Silicon Materials and Department of Materials Science and Engineering, Zhejiang University, Hangzhou 310027, P.R. China. Contact e-mail: cdgu@zju.edu.cn.

developed a citrate-EDTA bath that leads to high Mn content Zn-Mn alloys at low current densities. The ability of Zn-Mn alloys (Mn content between 0 and 15%) to resist atmospheric corrosion was tested by Soto (Ref 17), who reported a significant improvement in their corrosion performance in comparison with bare Zn or other Zn alloys.

Thus, many researchers have shown that Zn-Mn alloys with high Mn contents and monophasic crystal structures have an enhanced corrosion performance. In this respect, it has been suggested that high Mn content promotes the formation of a more compact passive layer made of Zn salts and Mn oxides, which suppresses anodic dissolution (Ref 7) and inhibits the cathodic reduction of dissolved oxygen (Ref 22). The presence of a monophasic structure has been shown to enhance corrosion resistance of Zn-Mn coatings by hindering the formation of local corrosion cells which may emanate in a two-phase structure due to phase differences (Ref 23). Besides the effects of chemical composition and crystal structure, the alloy crystallite size was also shown to play an important role in the corrosion behavior of Zn-Mn alloy coatings and it was shown that the corrosion resistance generally increases as the crystallite size decreases (Ref 23). Bucko et al. (Ref 24) observed that the corrosion resistances of monophasic Zn-Mn alloys decreases as their Mn content increases and their crystallite size increases, proving that high Mn content and a monophasic structure alone are not sufficient conditions for improving corrosion resistance.

Aprotic ionic liquids have proven to be good solvents for electrodeposition of metals, alloys, and semiconductors (Ref 25, 26), especially for very active elements, because the parallel hydrogen evolution reaction can be avoided. The electrodeposition of numerous Zn (Ref 27-31) alloys from ionic liquids has been reported. Deep eutectic solvents (DES) represent a class of ionic liquids and refer to the mixture of two solid compounds whose melting temperatures are usually above room temperature but when mixed together form a compound that has a melting point lower than room temperature. DES are formed from eutectic mixtures of a quaternary ammonium salt with a hydrogen bond donor species as a carboxylic acid, a glycol or an amine and are known for their ability to highly dissolve metal salts and oxides as well as organic materials such as cellulose. Choline chloride-based DES have been successfully assessed for electrodeposition of different metals (Cr, Mn, Cu, Ag, Fe, Zn) (Ref 32-38) and alloys (Zn/Cr, Zn/Sn, Zn/Ni, Zn-Mn, Ni-Co) (Ref 39-41) on different substrates producing films with characteristics that are completely different from those obtained from aqueous electrolytes.

The Zn-Mn alloys electrodeposited from ionic liquids are expected to be extremely superior in corrosion resistance compared to those from aqueous solutions, this is due to the numerous benefits afforded by ionic liquids such as avoidance of water chemistry defects and higher electrodeposition current efficiencies. Since, the standard electrode potentials of Zn^{2+}/Zn and Mn^{2+}/Mn couples are significantly far apart, various electrodeposition parameters must be regulated in order to achieve co-deposition of the less noble metal, Mn, with Zn. For example, it is known that the increase in electrolyte Mn^{2+} ion concentration shifts the deposition cathodic potential toward less negative value and this is beneficial for the increase in Mn% content in the alloy (Ref 42), while stirring or heating of the electrolyte leads to the opposite effect (Ref 43). Although an investigation has been done on the electrodeposition of Zn-Mn alloys from ionic liquids, no work has been reported with

regard to their characterization for corrosion protection. Thus, the corrosion behavior of Zn-Mn alloys with a variable Mn composition is worthy of being investigated systematically in search of Zn-Mn alloys of high corrosion resistance. In this paper, we present the morphology, composition, structure and corrosion performances of various Zn-Mn alloys obtained from a deep eutectic solvent by varying the electrodeposition potential and electrolyte Mn^{2+} concentration.

2. Experimental

### 2.1 Electrolyte Preparation and Electrochemical Testing

Choline chloride (ChCl) [$(HOC_2H_4N\ (CH_3)_3Cl)$] (Aldrich, 99%) was dried over night at 60 °C to remove moisture before use. Urea (U), zinc chloride [$ZnCl_2$] (Aldrich, >98%), and manganese (II) chloride ($MnCl_2.4H_2O$) (Aldrich, >99%) were used as obtained. The eutectic mixture was formed at 70 °C until a homogeneous colorless liquid was formed, by stirring the dried ChCl with the urea hydrogen bond donor mixture in a 2:1 molar ratio. The plating electrolytes were formed by adding appropriate quantities of manganese (II) chloride [$MnCl_2·4$-H_2O], zinc chloride [$0.4M ZnCl_2$], and boric acid [$0.4M\ H_3BO_3$] to the ChCl: 2U deep eutectic solvent and stirring the mixture at 70 °C until homogeneous electrolytes referred to as 0.4Zn-0.7Mn, 0.4Zn-1.0Mn, and 0.4Zn-1.4Mn henceforth in this paper and shown in Table 1 are obtained. Cyclic voltammetry (CV) experiments were carried out at 40 °C in a three-electrode system consisting of a platinum working electrode (1 cm^2), a platinum counter electrode and a silver reference electrode in a potential range of −1.8 to +0.5 V at 20 mV/s. To avoid Mn oxidation, each electrolyte was purged with 99.9% nitrogen gas for about fifteen minutes prior to cyclic voltammetry (CV) and during deposition a weak flux of N_2 was maintained. Before commencement of each experiment, the platinum electrodes were cleaned in nitric acid (HNO_3), rinsed in deionized water and dried. The conductivities of the electrolytes (Table 1) were determined at 40 °C using a portable DDBJ-350 conductivity meter (Leici, Shanghai) with a conductivity probe.

2.2 Electrodeposition and Coating Characterization

The main objective of this work was to optimize the Zn/Mn ratios and morphologies of the electrodeposited Zn-Mn films in order to obtain the films with the best corrosion resistance. In order to electrodeposit the exact ratio of Zn and Mn throughout the electrodeposition process, the potentiostatic method (voltage control) was chosen, since in the galvanostatic method (current control) there is a chance for potential fluctuation during deposition and this might lead to some changes in composition. The electrodeposition of Zn-Mn alloys performed at higher temperatures was very fast and could not produce thick, smooth, and adherent deposits. This could be due to the strong accelerating deposition effect at higher temperatures, so to avoid this problem we decided to perform our experiments at a lower temperature of 40 °C. Moreover, a lower temperature is good at enhancing Mn incorporation into the Zn-Mn films. For electrodeposition, a three-electrode cell with zinc anode, copper cathode (2 cm × 5 cm), and a silver reference electrode was used and a potentiostatic power supply was used. The cathode and anode were positioned parallel to each other with a gap distance of about 3 cm between them. The coatings were grown

Table 1 Electrolytes compositions

Component/M	A	B	C	D	E
H_3BO_3	0.4	0.4	0.4	…	…
$MnCl_2 \cdot 4H_2O$	0.7	1.0	1.4	0.7	…
$ZnCl_2$	0.4	0.4	0.4	…	0.4
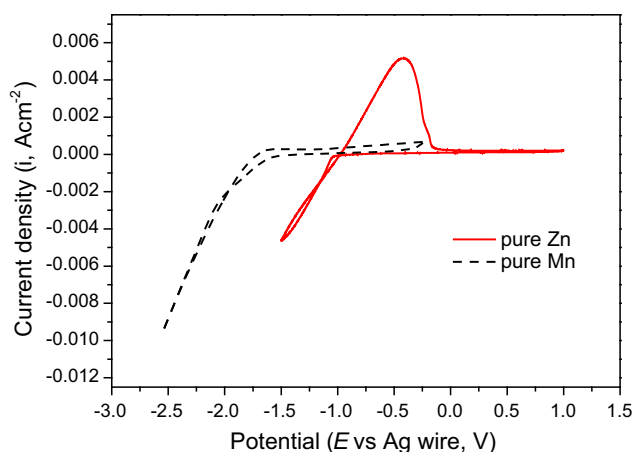
Fig. 1 Cyclic voltammograms pure 0.4M Zn and pure 0.7M Mn at 40 °C at a scan rate of 20 mV/s

potentiostatically at -1.6 and -1.8 V from each of the three electrolytes (Table 1) at 40 °C and electrodeposition time was adjusted to obtain deposits of the same thickness by maintaining the same electrodeposition charge density of 3C /cm^2 in each experiment. Before electrodeposition, the copper substrate was electrolytically cleaned in an alkaline solution (H_3PO_4 + Na_2CO_3 + NaOH) then subsequently rinsed in ethanol and deionised water, and dried. After electrodeposition of each film, the sample was thoroughly and simultaneously cleaned with ethanol and distilled water, and then dried in air. The surface morphologies of the deposits were observed by means of a scanning electron microscope (SEM). The attached liquid-nitrogen-cooled energy dispersive spectroscopy (EDS) detector was used to determine the chemical composition of the alloy and to confirm uniformity; each sample was analyzed at five different locations. Crystalline structures of the samples were studied by x-ray diffractometer (XRD).

The corrosion behaviors and protection performances of Zn-Mn alloy coatings were studied by the potentiodynamic polarization and electrochemical impedance spectroscopy (EIS) techniques in 3.5 wt.% NaCl solution using a classic three-electrode cell with a platinum plate as counter electrode, a Zn-Mn film (1 cm^2) as a working electrode and a saturated calomel electrode as reference. The exposed surface areas of the Zn-Mn films for testing were obtained using an insulating epoxy resin leaving an uncovered area of approximately 1 cm^2. EIS measurements were obtained at the open circuit potential (OCP) in a frequency range of 100 kHz-0.1 Hz, with an applied AC signal amplitude perturbation of 10 mV and the corresponding Nyquist plots were analyzed. Before each EIS experiment, the sample was first immersed into the 3.5 wt.% NaCl solution for approximately 4 h in order to establish a stable OCP. Then for the subsequent measurements of Tafel polarization curves, the polarization curve scanning rate was 1 mV/s, with a scanning range from -0.25 V of OCP to

$+0.50$ V of OCP. The corrosion current densities and corrosion potentials were determined based on Tafel's extrapolation.

3. Results and Discussion

3.1 Cyclic Voltammetry Study of Zn and Mn Electrodeposition

CV studies were performed to determine the electrochemical behaviors of individual Zn and Mn elements in their quiescent electrolytes (*D* and *E*) shown in Table 1. CV studies were carried out at a scan rate of 20 mV s^{-1} at 40 °C in all cases. The cyclic voltammetry curves shown in Fig. 1 represent the electrodeposition and stripping behavior of Zn/Zn^{2+} and Mn/Mn^{2+} species on a platinum electrode, respectively, where the potentials were initially scanned toward negative potentials. From Fig. 1, the reduction potential of Zn starts at approximately -1.04 V and the reduction peak is not well defined and the oxidation peak is positioned at around -0.4 V. For the Mn/Mn^{2+} species, Fig. 1 also shows no defined Mn reduction peak, but the cathodic current density rapidly increases when the potential is close to -1.6 V and this is due to the onset of Mn^{2+} ions reduction. It is important to note that for Mn/Mn^{2+} species, no anodic peak(s) is (are) observed during the potential scan in the positive direction. A similar behavior was reported by Ganesan et al. Ref 44 for 0.46MZn-(0.46-2.1) M Mn electrolytes and they attributed the absence of a peak potential to the instability of Mn deposits, which are easily dissolved back into the electrolyte.

3.2 Cyclic Voltammetry Study of Zn-Mn Deposition

Figure 2 gives the measured conductivities of the three Zn-Mn electrolytes (Table 1) and that of the pure deep eutectic solvent at 40 °C. It can be seen that the Zn-Mn electrolytes conductivities gradually increases with an increase in electrolyte Mn(II) concentration. The increase in electrolyte conductivities with an increase in Mn(II) concentration is due to increase in total metal ion concentration of the electrolytes. To study the electrochemical behaviors of Zn-Mn alloy electrodeposition from the three electrolytes (Table 1), CV studies were carried out in the potential range between -1.8 and $+0.5$ V at a scan rate of 20 mV s^{-1} and a temperature of 40 °C. Figure 3 shows the voltammograms of Zn-Mn electrolytes of different concentrations (Table 1), here it is observed that both Mn(II) and Zn(II) can be reduced to their metallic state, and that the reduction potentials of Mn(II) are observed at more negative potentials than those of Zn(II). During the potential scan in the negative direction, the deposition of Zn begins at a potential around -1.1 V and gives rise to a peak at a potential around -1.4 V. As the potential scan in the negative direction proceeds, another reduction peak is observed at a potential around -1.6 V. This result is in agreement with previously obtained results (Ref 45, 47) where it was shown that Mn electrodeposition occurs between -1.5 and -1.7 V. It is important to note that the reduction peak intensity of Zn increases with increase in electrolyte Mn(II) concentration and this may be related to increase in electrolyte conductivity as the total metal concentration in the electrolyte increases.

In addition, as the electrolyte Mn(II) content increases (Fig. 3), the reduction peaks for Mn are shifted in the positive direction whilst those of Zn are shifted in the negative direction,

this effect narrows the reduction gap between Zn and Mn thereby enhancing Mn incorporation into the Zn-Mn alloy deposit. The onset of reductions and reduction peaks of Zn
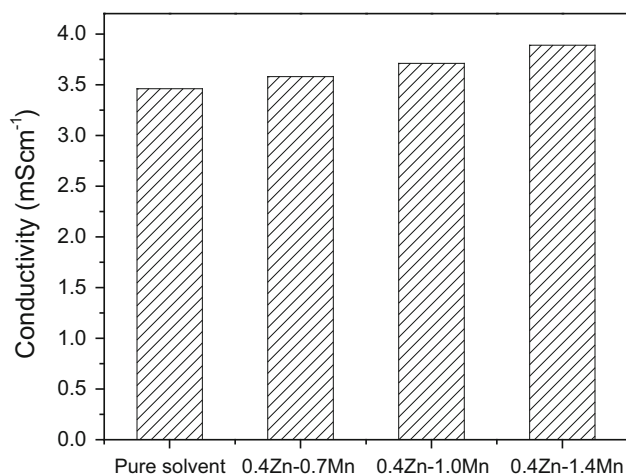

Fig. 2 Conductivity of 0.4Zn-0.7Mn, 0.4Zn-1.0Mn, and 0.4Zn-1.4Mn electrolytes at 40 °C
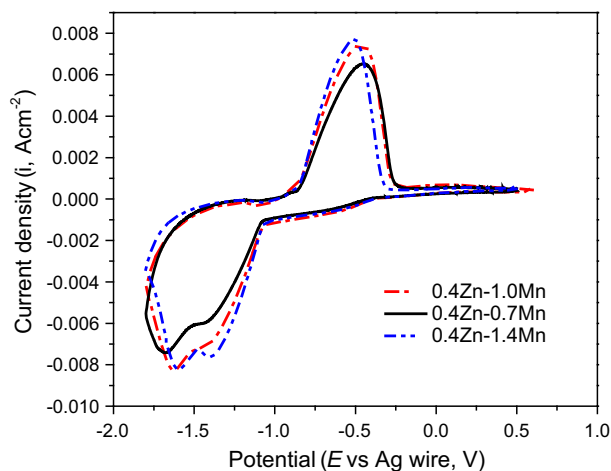

Fig. 3 Cyclic voltammograms of 0.4Zn-0.7Mn, 0.4Zn-1.0Mn, and 0.4Zn-1.4Mn electrolytes performed at 40 °C at a scan rate of 20 mV/s

from the Zn-Mn electrolytes are all more negative than that of pure Zn. It implies that the boric acid has a hindering effect on Zn electrodeposition and brings down the potential range for Zn-Mn co-deposition, thus enhancing the Mn incorporation into the deposit. When the potential scan is switched in the positive direction, only one oxidation peak occurs and it is displaced to more positive potentials with increase in Mn(II) concentration and this is likely to be due to incorporation of Mn into the Zn matrix. This suggests that the formed Mn phase during the negative potential scan is stable and accessible for electrochemical oxidation.

3.3 Deposits Morphology and Composition

Generally, the study of Zn-Mn electrodeposition is complicated due to the fact that Mn is readily oxidized (Ref 22), thus, in order to avoid Mn oxidation, nitrogen was purged into the electrolyte for about fifteen minutes prior to each electrodeposition experiment. Fig. 4(a) and (b) show the current (*i*)-time (*t*) curves recorded during potentiostatic electrodeposition from the three Zn-Mn electrolytes at deposition voltages of −1.6 and −1.8 V. It is clear that the currents for electrodeposition generally increase with increase in electrolyte total metal ion concentration in all cases and this is due to the increase in electrolyte conductivity. The currents of electrodeposition from the same electrolyte were higher at high electrodeposition potentials and lower at low electrodeposition potentials (Fig. 4a and b).

Visual examination of the Zn-Mn coatings indicated that bright and gray deposits were produced at low electrodeposition potentials and low electrolyte Mn(II) concentrations, and porous and darker deposits were electrodeposited at high electrodeposition potentials and high electrolyte Mn(II) concentrations. The differences in color may be attributed to different amounts of Mn contents in the deposits. The SEM micrographs (Fig. 5 and 6) show that the Zn-Mn electrodeposits, obtained at low electrodeposition voltages and low electrolyte Mn(II) concentrations, were homogeneous, compact, smooth, adherent, and shiny, and completely covered the substrate surface. With increase in electrodeposition potential and electrolyte Mn(II) content (Fig. 5a-c and 6a-c), the morphologies of the electrodeposits varied from coarse grains to fine and rough grains indicating that incorporation of small quantities of Mn into Zn matrices significantly alters the surface morphology of the Zn-Mn alloys. According to the electro-crystallization theory, metal atoms generated by the discharge
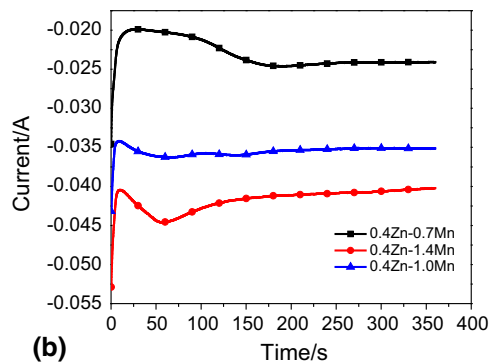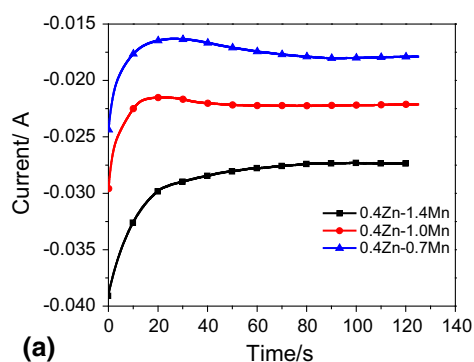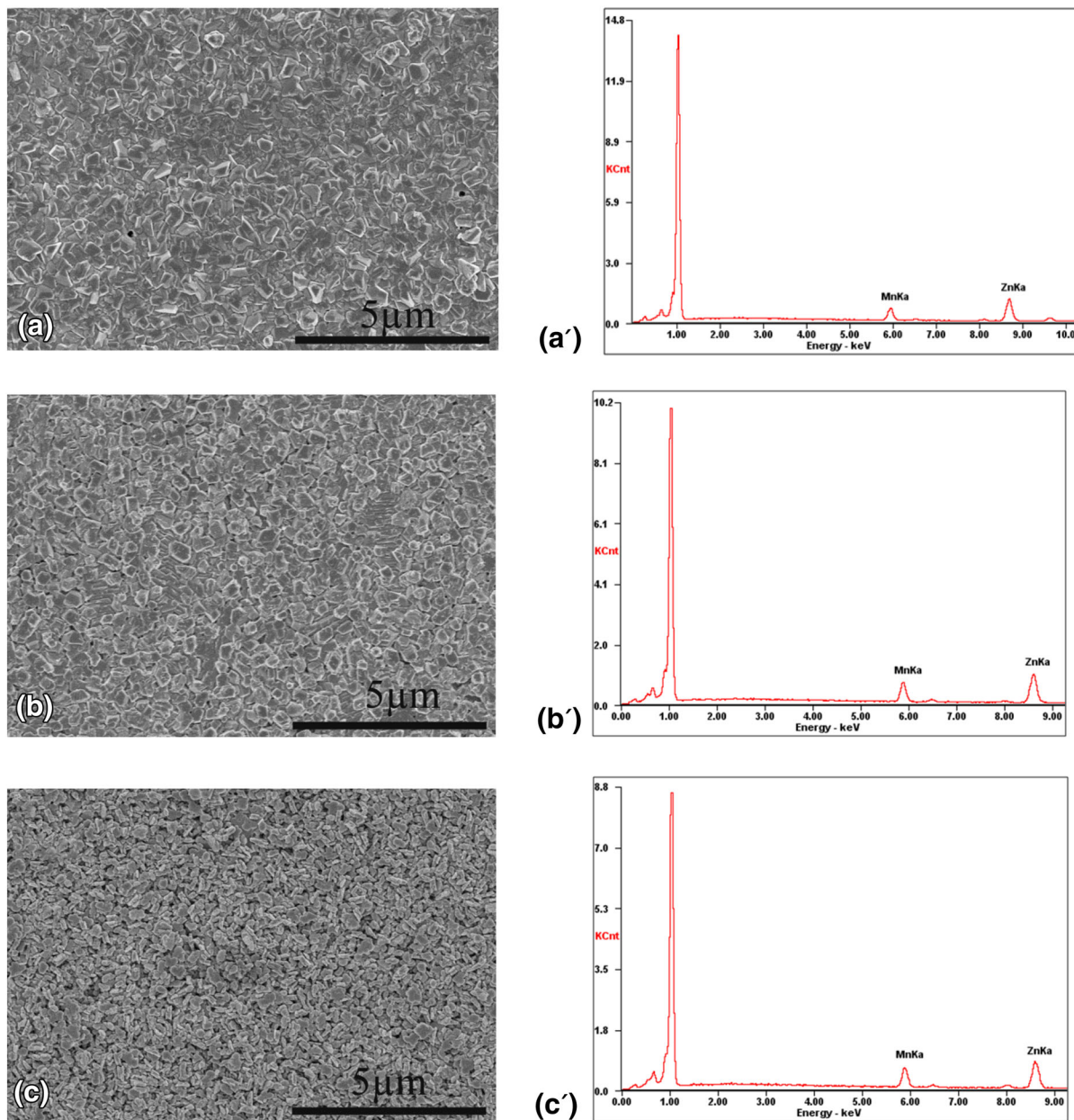

Fig. 4 Effect of electrodeposition potential on the electrodeposition current vs. time of 2 cm × 5 cm copper electrodes from Zn-Mn electrolytes (Table 1) elecrodeposited at (a) −1.6 V and (b) −1.8 V

Fig. 5 Surface morphologies (SEM) of the electrodeposited Zn-Mn films from (a) 0.4Zn-0.7Mn, (b) 0.4Zn-1.0Mn, and (c) 0.4Zn-1.4Mn electrolytes at −1.6 V, 40 °C and their corresponding EDS analysis (a′, b′, c′)

of metal ions on the cathode may either be incorporated into the crystals and thus promote crystal growth, or may form a new nucleus when the rate of crystal growth is not sufficient to accept new atoms (Ref 51). So, the number of newly formed nuclei will increase, whereas their radii decrease with the increase in deposition overpotential (Ref 49). Thus, in this case the increase in electrodeposition potential (fast electrodeposition rate) leads to a decrease in the film crystallite size and appearance of a rough and porous morphology.

Figure 5 and 6 show the EDS patterns of Zn-Mn deposits obtained by potentiostatic electrodeposition from the three electrolytes (Table 1) at 40 °C, where it is observed that all the obtained Zn-Mn deposits contain both Zn and Mn. The variations of Mn contents in these alloys as a function of electrolyte composition and electrodeposition potential are shown in Fig. 7. Increasing the electrodeposition voltages and electrolyte Mn(II) concentrations increased the Mn content in the Zn-Mn deposits. The co-deposition of Zn and Mn is normal, which means that Mn content in the Zn-Mn alloy will increase with the increase in deposition voltage and this is in strong agreement with our results shown in Fig. 7. A significant increase in Mn content indicates that the deposition potential is reached where Zn reduces at diffusion limiting potential, so further change of
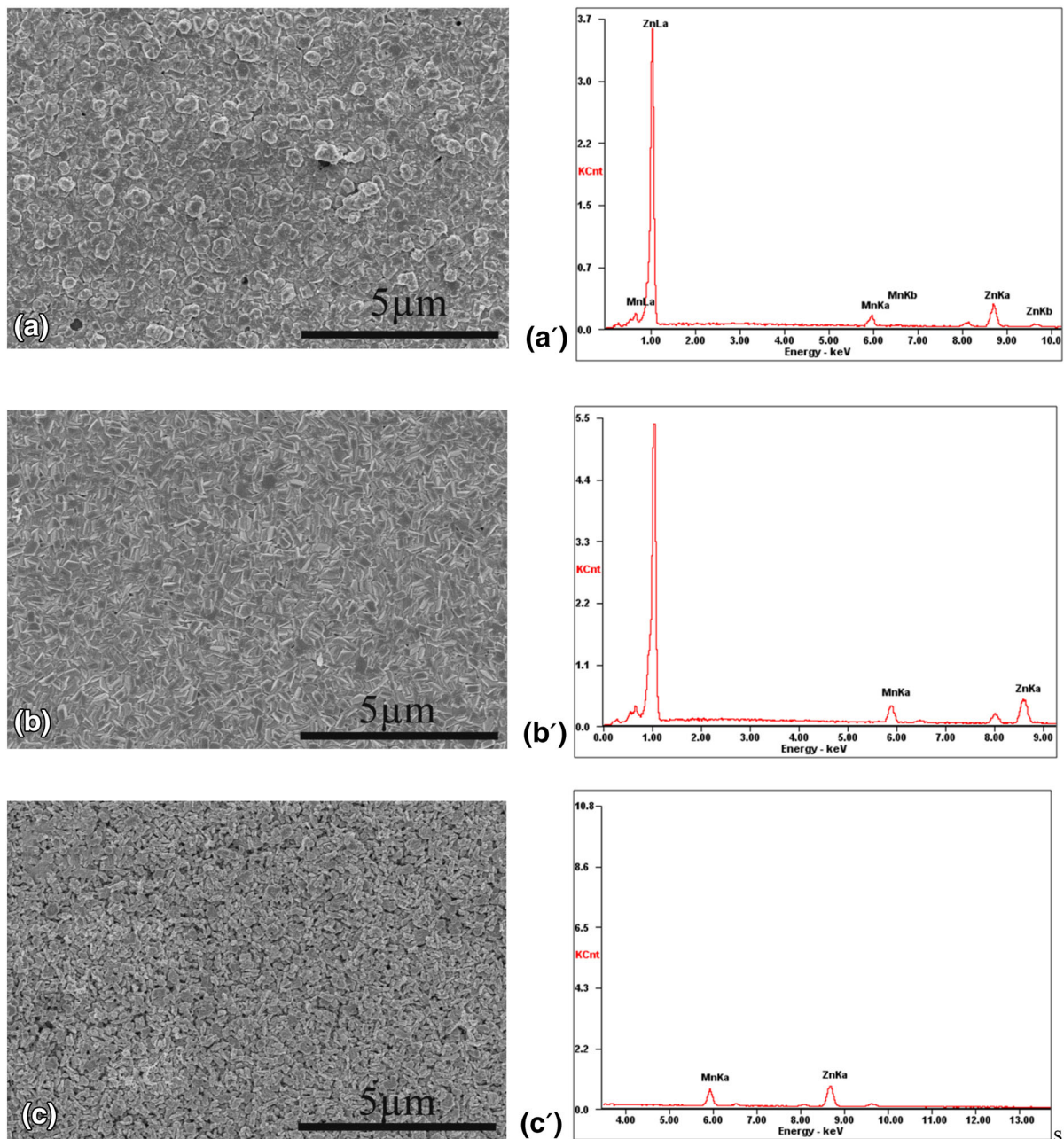
Fig. 6 Surface morphologies (SEM) of the electrodeposited Zn-Mn films from (a) 0.4Zn-0.7Mn, (b) 0.4Zn-1.0Mn, and (c) 0.4Zn-1.4Mn electrolytes at −1.8 V, 40 °C and their corresponding EDS analysis (a′, b′, c′)

deposition potential to the negative values enhances only the Mn deposition (Ref 46).

3.4 Phase Structure of Deposits

The crystal structure of the deposited Zn-Mn alloy coatings was analyzed by XRD. Usually, the observed Zn-Mn phases essentially depends on the Mn content in the alloy (Ref 44) and the variation of plating parameters such as stirring and temperature only affect the relative intensity of the peaks. The x-ray diffraction patterns of Zn-Mn samples deposited from the three electrolytes (Table 1) at (a) −1.6 V (Fig. 8a, c and e) and (b) −1.8 V (Fig. 8b, d and f) are shown in Fig. 8(a-f), respectively. The Zn-Mn phases were identified by analysis of the peak positions and comparing them with structural parameters obtained from literature (Ref 50). The crystal structures of Zn-Mn deposits consisted of Zn and hexagonal close packed ε-phase Zn-Mn at low electrodeposition potentials and low electrolyte Mn(II) content (Fig. 8a and b) and this might be due to high alloy Zn contents in relation to Mn contents. However, at high electrodeposition potentials and high electrolyte Mn(II) contents, only hexagonal close packed ε-phase of Zn-Mn alloy was
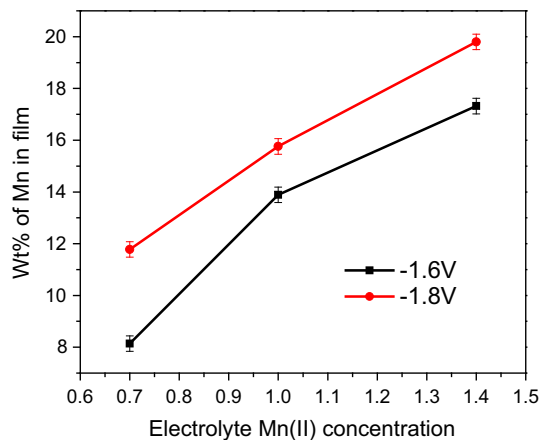
Fig. 7 Variation of Mn content of electrodeposited Zn-Mn films with electrolyte Mn(II) concentration at, (a) −1.6 V and (b) −1.8 V

obtained (Fig. 8e and f) and this might be due to low Zn contents in relation to Mn contents. The presence of monophasic ε-Zn-Mn phase at high Mn contents is beneficial from the point of corrosion application, because it has been documented that single-phase Zn-Mn coatings possess higher corrosion resistance as compared to the two-phase deposits and in addition the ε-phase has the highest stability against corrosion (Ref 47).

3.5 Corrosion Resistance Measurements

3.5.1 Potentiodynamic Polarization Studies. To evaluate the corrosion resistances of the Zn-Mn alloys, coatings deposited under different potentials and electrolyte Mn(II) concentrations were prepared on copper electrodes and were covered to expose a geometric surface area of 1 cm². The corrosion resistances of the deposits were evaluated by polarization measurements using a 3.5 wt.% NaCl solution, which is an appropriate media for studying corrosion due to the
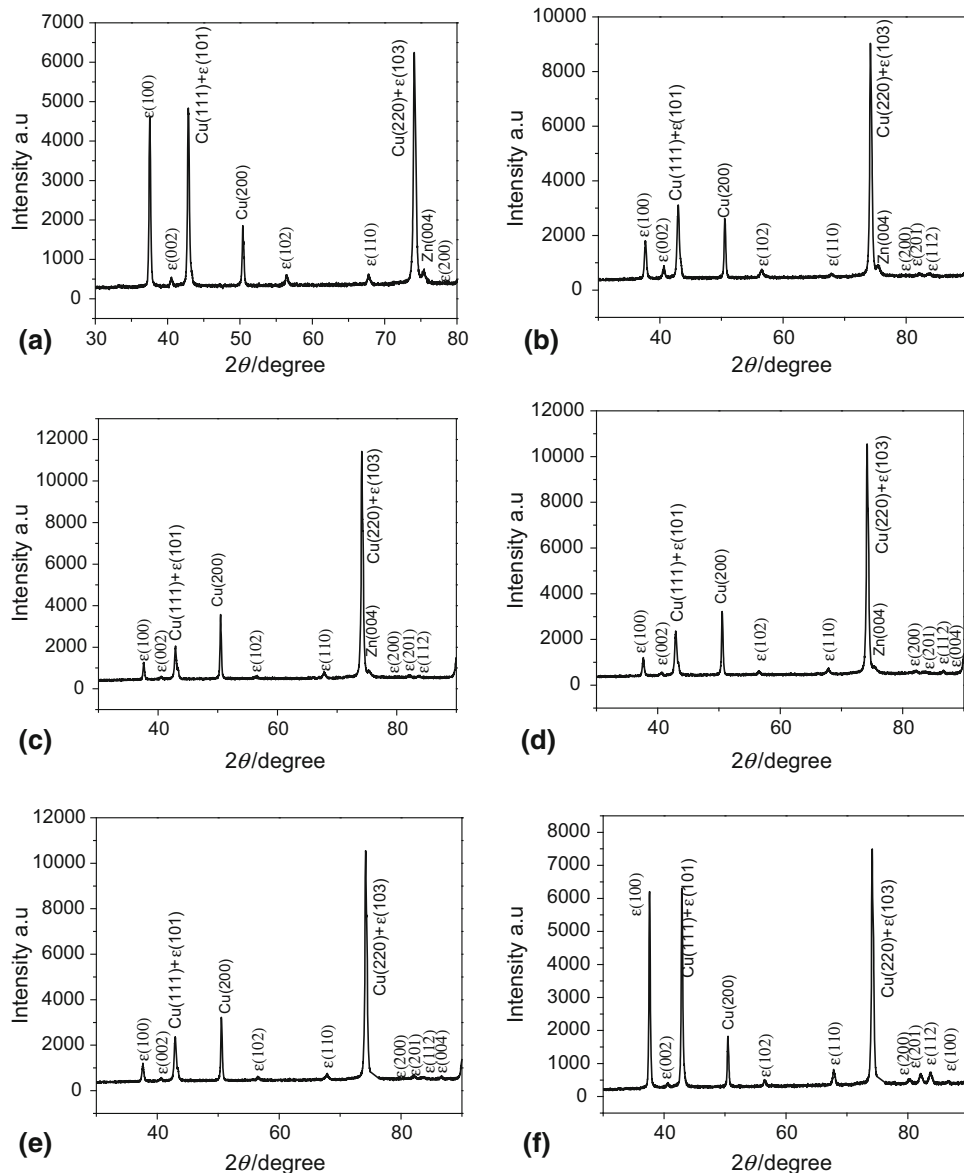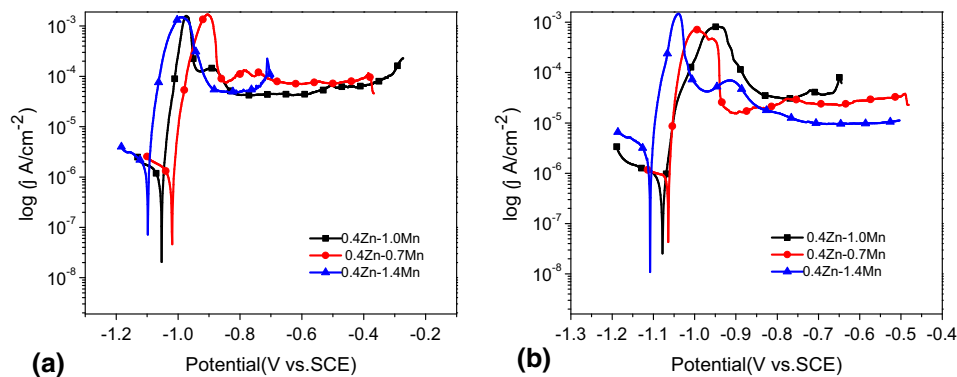

Fig. 8 X-ray diffraction patterns of Zn-Mn samples deposited from 0.4Zn-0.7Mn, 0.4Zn-1.0Mn and 0.4Zn-1.4Mn electrolyte at −1.6 V (a, c, e) and −1.8 V (b, d, f), respectively, at 40 °C

Fig. 9 Potentiodynamic polarization curves of Zn-Mn samples deposited from 0.4Zn-0.7Mn, 0.4Zn-1.0Mn, and 0.4Zn-1.4Mn electrolytes at, (a) −1.6 V and (b) −1.8 V, 40 °C

Table 2 Corrosion characteristics, obtained by polarization in 3.5 wt.% NaCl solution, of the Zn-Mn samples obtained at −1.6 and −1.8 V from 0.4Zn-0.7Mn, 0.4Zn-1.0Mn, and 0.4Zn-1.4Mn electrolytes at 40 °C

Film	Corrosion potential, E_{corr}/mV	Corrosion current density, i_{corr}/µAcm^{-2}	Solution resistance, R_s(Ωcm^2)	Polarization resistance, R_p (Ωcm^2)
A$_{-1.6\ V}$	−1021	1.075	5.2	5456
B$_{-1.6\ V}$	−1054	0.917	4.5	7060
C$_{-1.6\ V}$	−1098	1.175	4.7	2116
A$_{-1.8\ V}$	−1062	0.989	4.6	5521
B$_{-1.8\ V}$	−1079	0.875	4.3	7577
C$_{-1.8\ V}$	−1109	1.251	3.9	1300

presence of corrosion activators (chloride ions). Figure 9(a) and (b) show the potentiodynamic polarization curves obtained. Table 2 show the results obtained from the Tafel evaluation of the corrosion parameters of the coatings from Fig. 9(a) and (b), where the letter represent the electrolyte from which the film was electrodeposited from and the subscript represent the electrodeposition potential. It can be seen that the corrosion potential, E_{corr} for the electrodeposited Zn-Mn alloys shifts to more negative potentials with an increase in the alloy Mn content. These results show that the incorporation of Mn into Zn matrices further sacrifically inhibits the corrosion of the underlying substrate in aggressive environments since the corrosion potentials of all the Zn-Mn alloys are more negative than that of steel [−640 mV (Ref 48)]. Thus, all of the tested coatings can provide a certain degree of galvanic or sacrificial protection to the steel substrate.

The potentiodynamic polarization curves (Fig. 9a and b) of Zn-Mn deposits show three different processes: active disso-lution, passivation, and trans-passivation region. In active dissolution region, the current density rapidly increases after the corrosion potential with a potential change in the positive direction until the passivation region is reached. Then a passivation region is entered where a passive film formation occurs on the surface. The presence of this film inhibits metal dissolution process resulting in a decrease in current density. Then the final region is when the breaking of the passive film occurs at higher potentials and the corrosion potential reaches that of the substrate due to exposure of the underlying substrate. The copper substrates used here have low corrosion currents such that the corrosion currents remain low after the breakage of the passive film. The passive barrier layer slows down the

diffusion of the corrosive species and thus slows down the corrosion process. Generally, such a barrier layer forms when dissolution of the metal causes the concentration of metal ions near the electrode surface to exceed the solubility constant of the salt comprised of the metal ions and anionic species in the adjoining solution, causing a solid film to form. XRD and XPS studies by Boshkov (Ref 7-9) showed that in the case of Zn-Mn alloys, the passive film is formed by the zinc hydroxide chloride compound Zn $(OH)_{1.6}Cl_{0.4}$(ZHC) with a very low solubility product.

The corrosion behavior of Zn-Mn alloys is strongly affected by two independent factors, i.e., chemical/phase composition and surface morphology. The corrosion currents shown in Table 2 show that the corrosion resistances of the Zn-Mn alloys first increases with increase in Mn content and this is due to the presence of a single ε-Zn-Mn phase at higher Mn content on one hand. Secondly, higher Mn content promotes the formation of more compact passive layer made of Zn salts and various Mn oxides, which suppresses the anodic dissolution (Ref 7). These oxides have been reported to inhibit the cathodic reduction of dissolved oxygen (Ref 22). This is in agreement with literature data which showed that there was an increase in the corrosion resistance of Zn-Mn electrodeposits as the crystallite size decreased (Ref 24). The challenge experienced with small crystallites at very high electrodeposition potentials and very high electrolyte Mn(II) concentration is the formation of pores producing a rough and non-homogeneous morphology. Thus, the reason why coatings with a highest Mn content exhibited lower corrosion resistance is that they had some pores. According to literature (Ref 51, 52), the deposit morphology has a stronger effect to corrosion resistance than its composi-
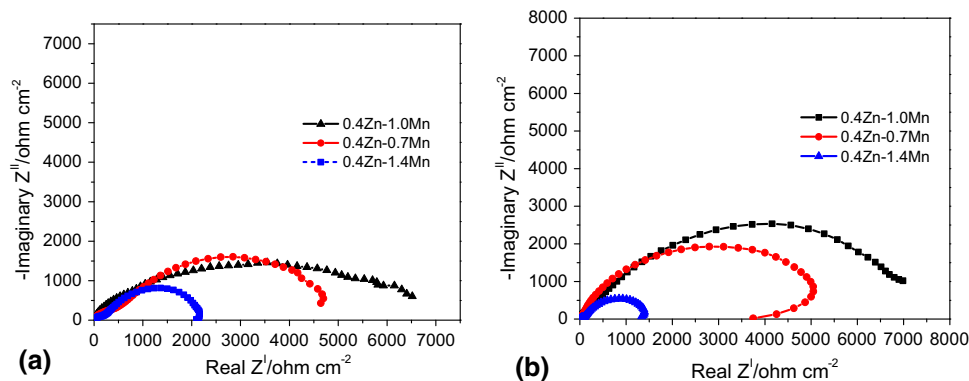
Fig. 10 Nyquist plots of Zn-Mn films electrodeposited at (a) −1.6 V and (b) −1.8 V from 0.4Zn-0.7Mn, 0.4Zn-1.0Mn and 0.4Zn-1.4Mn electrolytes at 40 °C

tion. This shows that for good corrosion performance a combination of a sufficiently high Mn content and a good morphology are necessary. Under the conditions considered, a Zn-Mn alloy coating deposited from 0.4Zn-1.0Mn electrolyte at a potential of −1.8 V showed the lowest corrosion current density (i_{corr}) value among all Zn-Mn deposits investigated here (Table 2).

3.6 Electrochemical Impedance Spectroscopy

Electrochemical impedance spectroscopy (EIS) is a versatile non-destructive technique in which a small oscillating perturbation in cell potential is applied to an electrochemical system for identifying the corrosion mechanisms and kinetics, which are not usually observable by potentiodynamic polarization studies. Nyquist plots are commonly used to illustrate the relative tendency of coatings undergoing corrosion with the provision to distinguish the contribution of polarization resistance (R_p) versus solution resistance (R_s). EIS studies were carried out on all the Zn-Mn coatings after 4 h of continuous immersion into the 3.5 wt.% NaCl solution. Figure 10 show the EIS spectrum (Nyquist plots) of the Zn-Mn alloys (deposited at −1.6 and −1.8 V) in 3.5 wt.% NaCl solution, showing the real (Z_{real}) and imaginary (Z_{img}) parts of the measured impedance. The real parts of the impedance of the samples are significantly bigger than the imaginary parts. This can be attributed to the charge transfer resistance control of the corrosion reactions of the samples because of the domination of the Zn-rich phases in the coatings. The Nyquist plots of Zn-Mn coatings exhibit two time constants, which are characterized by the appearance of two depressed semi circles. The high-frequency time constants could thus be attributed to the formation of corrosion products, while the low-frequency time constants should be related to the activation process. At low frequency limit all the electrochemical cells tend to exhibit the inductive behavior; characterized by the decrease of both Z_{real} and Z_{img}. This explains the adsorption phenomena of the Zn-Mn coatings. The corrosion (polarization) resistances of the coatings are related to the impedance diameter where a semicircle with larger diameters indicates high corrosion resistance coatings (Ref 53). As seen in Fig. 10(a) and (b) the semicircle diameter of the film electrodeposited from the 0.4Zn-1.0Mn electrolyte at −1.8 V is the biggest and that of the film electrodeposited from the 0.4Zn-1.4Mn electrolyte at −1.8 V is the smallest. The

solution resistances (R_s) and the polarization resistances (R_P) were obtained through the use of Z-view analyzing software and their values are shown in Table 2. The solution resistances were almost the same since the same solution was used in all impedance tests. The polarization resistances show that the highest corrosion resistance was obtained from the coating electrodeposited at −1.8 V from the 0.4Zn-1.0Mn electrolyte. These obtained corrosion behaviors of the Zn-Mn coatings are consistent with those obtained from the potentiodynamic polarization studies and are higher than those normally obtained from aqueous electrolytes (Ref 44).

4. Conclusions

This study examined the morphologies, compositions, and corrosion resistances of Zn-Mn alloy coatings obtained from deep eutectic solvent-based electrolytes under different electrodeposition potentials and electrolyte Mn(II) compositions with boric acid as an additive. The characterization results have shown that the Mn content of the Zn-Mn alloys increases with increase in electrodeposition potential and electrolyte Mn(II) composition. The SEM study shows that the coatings morphology becomes finer, rough, and porous at higher electrodeposition potentials and high electrolyte Mn(II) concentrations. The crystal structure of Zn-Mn deposits consists of Zn and hexagonal close packed ε-phase Zn-Mn at low electrodeposition potentials and low electrolyte Mn(II) contents. However, at high electrodeposition potentials and electrolyte Mn(II) contents, the crystal structure was only composed of hexagonal close packed ε-phase Zn-Mn. The corrosion testing of the samples showed that they have a passivating behavior and their corrosion performance depends strongly on their composition (chemical and phase) and morphology. The Zn-Mn films deposited from 0.4Zn-1.0Mn electrolyte at −1.8 V showed the best corrosion resistance and this was attributed to a sufficiently high Mn content, a smooth morphology and a monophasic phase structure.

References

1. G.D. Wilcox and D.R. Gabe, Electrodeposited Zinc Alloy Coatings, *Corros. Sci.*, 1993, **35**, p 1251–1258

2. D.R. Gabe, G.D. Wilcox, A. Jamani, B.R. Pearson, Zinc-Manganese Alloy Electrodeposition, *Met. Finish.*, 1993, **91**, p 34–36

3. G.D. Wilcox and B. Petersen, Zinc-Manganese Alloy Electrodeposition, *Trans. Inst. Met. Finish.*, 1996, **74**, p 115–118

4. K.N. Srinivasan, M. Selvan, and K.I.S. Venkata, Hydrogen Permeation During Zinc-Manganese Alloy Plating, *J. Appl. Electrochem.*, 1993, **23**, p 358–363

5. M. Sagiyama, T. Urakawa, T. Adaniya, T. Hara, and Y. Fukuda, Zinc-Manganese Alloy Electroplating on Steel Strip, *Plat. Surf. Finish.*, 1987, **74**, p 40

6. N. Boshkov, K. Petrov, S. Vitkova, and G. Raichevsky, Galvanic Alloys Zn-Mn—Composition of the Corrosion Products and their Protective Ability in Sulfate Containing Medium, *Surf. Coat. Technol.*, 2005, **194**, p 276–282

7. N. Boshkov, K. Petrov, D. Kovacheva, S. Vitkova, and S. Nemska, Influence of the Alloying Component on the Protective Ability of Some Zinc Galvanic Coatings, *Electrochim Acta*, 2005, **51**, p 77–84

8. N. Boshkov, Galvanic Zn-Mn Alloys-Electrodeposition, Phase Composition, Corrosion Behavior and Protective Ability, *Surf. Coat. Technol.*, 2003, **172**, p 217–226

9. N. Boshkov, K. Petrov, and G. Raichevsky, Corrosion Behavior and Protective Ability of Multilayer Galvanic Coatings of Zn and Zn-Mn Alloys in Sulfate Containing Medium, *Surf. Coat. Technol.*, 2005, **200**, p 5995–6001

10. G. Govindarajan, V. Ramakrishnan, S. Ramamurthi, V. Subramanian, and N.V. Parthasaradhy, Electrodeposition of Zinc-Manganese Alloy Coating for Corrosion Resistant Applications, *Bull. Electrochem.*, 1989, **5**, p 422–426

11. T. Urakawa, M. Sagiyama, T. Adaniya, T. Hara, *Corrosion-Resistance and Paintability of Zn-Mn Alloy Plated Steel Sheets*, SAE Tech 860268, 1986

12. M. Eyraud, A. Garnier, F. Mazeron, and Crousier, Morphology and Composition of Electrodeposited Zinc-Manganese Alloys, *J. Plat. Surf. Finish.*, 1995, **82**, p 63–70

13. M.V. Ananth and N.V. Parthasaradhy, Magnetization Behaviour of Electrodeposited Zn-Mn Alloys, *Mater. Sci. Eng.*, 1996, **40**, p 19–23

14. M. Selvam and S. Guruviah, Corrosion of Electrodeposited Zinc-Manganese Alloys, *Bull. Electrochem.*, 1990, **6**, p 485–486

15. B. Bozzini, F. Pavan, G. Bollini, and P.L. Cavallotti, Zn-Mn Alloy Electrodeposition on Steel, *Trans. Inst. Met. Finish.*, 1997, **75**, p 175–180

16. B. Bozzini, F. Pavan, and P.L. Cavallotti, Experience with a Pilot Plant for the Electrodeposition of Zn-Mn on Wire, *Trans. Inst. Met. Finish.*, 1998, **76**, p 171–178

17. F. Soto, *Electrodeposition of Zn-Mn Alloys on Steel for Corrosion Resistance*, Ph.D. Thesis, Universite de Provence, Aix Marseille 1, 1998

18. N. Boshkov, S. Vitkova, and K. Petrov, Corrosion Products of Zn-Mn Coatings: Part I. Investigations Using Microprobe Analysis and X-Ray Diffraction, *Met. Finish.*, 2001, **99**, p 56–60

19. N. Boshkov, K. Petrov, and S. Vitkova, Corrosion Products of Zn-Mn Coatings: Part III. Double-protective Action of Manganese, *Met. Finish.*, 2002, **100**, p 98–102

20. C. Muller, M. Sarret, and T. Andreu, Electrodeposition of Zn-Mn Alloys at Low Current Densities, *J. Electrochem. Soc.*, 2002, **149**, p C600–C606

21. C. Muller, M. Sarret, and T. Andreu, Zn-Mn Alloys Obtained Using Pulse, Reverse and Superimposed Current Modulations, *Electrochim. Acta*, 2003, **48**, p 2397–2404

22. L.D. Ballote, R. Ramanauskas, and P.B. Perez, Mn Oxide Film as Corrosion Inhibitor of Zn-Mn Coatings, *Corros. Rev.*, 2000, **18**, p 41–51

23. M.S. Chandrasekara and M. Shanmugasigamani, Synergetic Effects of Pulse Constraints and Additives in Electrodeposition of Nanocrystal-line Zinc: Corrosion, Structural and Textural Characterization, *Mater. Chem. Phys.*, 2010, **124**, p 516–528

24. M. Bucko, J. Rogan, S.I. Stevanovic, S. Stankovic, and J.B. Bajat, The Influence of Anion Type in Electrolyte on the Properties of Electro-deposited Zn\Mn Alloy Coatings, *Surf. Coat. Technol.*, 2013, **228**, p 221–228

25. F. Endres, Ionic Liquids: Solvents for the Electrodeposition of Metals and Semi-Conductors, *ChemPhysChem*, 2002, **3**, p 144–154

26. S.Z. EI Abedin, F. Endres, Electrodeposition of Metals and Semiconductors in Air- and Water-stable Ionic Liquids, ChemPhysChem, 2006, **7**, p 58–61

27. J.F. Huang and I.W. Sun, Nonanomalous Electrodeposition of Zinc-Iron Alloys in an Acidic Zinc Chloride-1-Ethyl-3-Methylimidazolium Chloride Ionic Liquid, *J. Electrochem. Soc.*, 2004, **151**, p C8–C14

28. J.F. Huang and I.W. Sun, Electrochemical Studies Tin in Zinc Chloride-1-Ethyl-3-Methylimidazolium Chloride Ionic Liquids, *J. Electrochem. Soc.*, 2003, **150**, p E299–E306

29. M.C. Lin, P.Y. Chen, and I.W. Sun, Electrodeposition of Zinc Telluride from a Zinc Chloride-1-Ethyl-3-Methylimidazolium Chloride Molten Salt, *J. Electrochem. Soc.*, 2001, **148**, p C653–C658

30. P.Y. Chen and I.W. Sun, Electrodeposition of Cobalt and Zinc-Cobalt from a Lewis Acidic Zinc Chloride-1-Ethyl-3-Methylimidazolium Chloride Molten Salt, *Electrochim. Acta*, 2001, **46**, p 1169–1177

31. J.F. Huang and I.W. Sun, Electrodeposition of Pt-Zn in a Lewis Acidic $ZnCl_2$-1-Ethyl-3-Methylimidazolium Chloride Ionic Liquid, *Electro-chim. Acta*, 2004, **49**, p 3251–3258

32. A.P. Abbott, G. Capper, D. Davies, and R.K. Rasheed, Ionic Liquid Analogues Formed from Hydrated Metal Salts, *Chem. Eur. J.*, 2004, **10**, p 3769–3774

33. A.P. Abbott, K. El Ttaib, G. Grish, K.J. McKenzie, and K.S. Ryder, Electrodeposition of Copper Composites from Deep Eutectic Solvents Based on Choline Chloride, *Phys. Chem. Chem. Phys.*, 2009, **11**, p 4269–4277

34. R. Bock and S.E. Wulf, Electrodeposition of Iron Films from an Ionic Liquid (ChCl/urea/$FeCl_3$ Deep Eutectic Mixtures, *Trans. Inst. Met. Finish.*, 2009, **87**, p 28–32

35. A. Bakkar and V. Neubert, Electrodeposition onto Magnesium in Air and Water Stable Ionic Liquids: From Corrosion to Successful Plating, *Electrochem. Commun.*, 2007, **9**, p 2428–2435

36. C.D. Gu, Y.H. You, Y.L. Yu, S.X. Qu, J.P. Tu Microstructure, Nanoindentation, and Electrochemical Properties of the Nanocrystal-line Nickel Film Electrodeposited from Choline Chloride-Ethylene Glycol, *Surf Coat. Technol.*, 2011, **205**, p 4928–4933

37. C.D. Gu and J.P. Tu, Fabrication and Wettability of Nanoporous Silver Film on Copper from Choline Chloride-Based Deep Eutectic Solvents, *J. Phys. Chem.*, 2010, **114**, p 13614–13619

38. S. Fashu, C.D. Gu, X.L. Wang, and J.P. Tu, Influence of Electrode-position Conditions on the Microstructure and Corrosion Resistance of Zn-Ni Alloy Coatings from a Deep Eutectic Solvent, *Surf. Coat. Technol.*, 2014, **242**, p 34–41

39. A.P. Abbott, G. Capper, K. Mckenzie, and K. Ryder, Electrodeposition of Zinc-Tin Alloys from Deep Eutectic Solvents Based on Choline Chloride, *J. Electroanal. Chem.*, 2007, **599**, p 288–294

40. P. Dale, A. Samantilleke, D. Shivagan, and L. Peter, Synthesis of Cadmium and Zinc Semiconductor Compounds from an Ionic Liquid Containing Choline Chloride and Urea, *Thin Solid Films*, 2007, **515**, p 5751–5754

41. H.Y. Yang, X.W. Guo, X.B. Chen, S.H. Wang, G.H. Wu, W.J. Dingb, and N. Birbilis, On the Electrodeposition of Nickel-Zinc Alloys from a Eutectic-Based Ionic Liquid, *Electrochim. Acta*, 2012, **63**, p 131–138

42. Y.H. You, C.D. Gu, X.L. Wang, and J.P. Tu, Electrodeposition of Ni-Co Alloys from a Deep Eutectic Solvent, *Surf. Coat. Technol.*, 2012, **206**, p 3632–3638

43. C. Savall, C. Rebere, D. Sylla, M. Gadouleau, Ph Refait, and J. Creus, Morphological and Structural Characterisation of Electrodeposited Zn-Mn Alloys from Acidic Chloride Bath, *Mater. Sci. Eng. A*, 2006, **430**, p 165–171

44. S. Ganesan, G. Prabhu, and B.N. Popov, Electrodeposition and Characterization of Zn-Mn Coatings for Corrosion Protection, *Surf. Coat. Technol.*, 2014, **238**, p 143–151

45. D. Sylla, C. Rebere, M. Gadouleau, C. Savall, J. Creus, and Ph Refait, Electrodeposition of Zn-Mn Alloys in Acidic and Alkaline Baths, Influence of Additives on the Morphological and Structural Properties, *J. Appl. Electrochem.*, 2005, **35**, p 1133–1139

46. D. Sylla, J. Creus, C. Savall, O. Roggy, M. Gadouleau, and Ph Refait, Electrodeposition of Zn-Mn Alloys on Steel from Acidic Zn-Mn Chloride Solutions, *Thin Solid Films*, 2003, **424**, p 171–178

47. M. Farzaneh, K. Raeissi, and M. Golozar, Effect of Current Density on Deposition Process and Properties of Nanocrystalline Ni-Co-W Alloy Coatings, *J. Alloys Compd.*, 2010, **489**, p 488–492

48. R. Ramanauskas, Structural Factor in Zn Alloy Electrodeposit Corrosion, *Appl. Surf. Sci.*, 1999, **153**, p 53–64

49. S. Tezuka, S. Sakai, and Y. Nakagawa, Ferromagnetism of Mn-Zn Alloy, *J. Phys. Soc. Jpn.*, 1960, **15**, p 931

50. Y. Nakagawa and T. Hori, Neutron Diffraction Studies of Mn-Zn Alloys, *J. Phys. Soc. Jpn.*, 1964, **19**, p 2082–2087

51. M.V. Tomic, M.M. Bucko, M.G. Pavlovic, and J.B. Bajat, Corrosion Stability of Electrochemically Deposited Zn-Mn Alloy Coatings, *Contemp. Mater.*, 2010, **1**, p 1

52. R. Ramanauskas, L. Gudaviciute, R. Juskenas, and O. Scit, Structural and Corrosion Characterization of Pulse Plated Nanocrystalline Zinc Coatings, *Electrochim. Acta*, 2007, **53**, p 1801–1810

53. A.C. Hegde, K. Venkatakrishna, and N. Eliaz, Electrodeposition of Zn-Ni, Zn-Fe and Zn-Ni-Fe Alloys, *Surf. Coat. Technol.*, 2010, **205**, p 2031–2041